



Article

Adsorption of Myelin Basic Protein on Model Myelin Membranes Reveals Weakening of van der Waals Interactions in a Lipid Ratio-Dependent Manner

Petra Maleš ¹, Barbara Pem ¹, Dražen Petrov ², Agustín Mangiarotti ³, Rumiana Dimova ³ and Danijela Bakarić ^{1,*}

- Division of Organic Chemistry and Biochemistry, Ruder Bošković Institute, Bijenička 54, 10000 Zagreb, Croatia; petra.males94@gmail.com (P.M.); barbara.pem@irb.hr (B.P.)
- Institute of Molecular Modeling and Simulation, University of Natural Resources and Life Sciences, 1180 Vienna, Austria; drazen.petrov@boku.ac.at
- Max Planck Institute of Colloids and Interfaces, Science Park Golm, 14476 Potsdam, Germany; agustin.mangiarotti@gmail.com (A.M.); rumiana.dimova@mpikg.mpg.de (R.D.)
- * Correspondence: danijela.bakaric@irb.hr; Tel.: +385-1-4571-382

Abstract

Myelin is a lipid-rich membrane that insulates axons, providing support and ensuring efficient nerve impulse conduction. Disruption of this sheath, or demyelination, impairs neural transmission and underlies symptoms like vision loss and muscle weakness in multiple sclerosis (MS). Despite extensive studies using in vitro and in vivo models, the molecular mechanisms driving demyelination remain incompletely understood. To investigate the role of myelin basic protein (MBP) in membrane stability, we prepared model myelin membranes (MMMs) from lipids expectedly undergoing gel-to-fluid phase transition, mimicking both normal and altered myelin, with and without MBP. Differential scanning calorimetry (DSC) revealed that MBP suppresses the main phase transition in normal MMMs, unlike in modified MMMs. FTIR spectra showed strengthening of van der Waals interactions in normal MMMs with MBP upon heating and opposite effects in the analogous modified MMM system. Additionally, phosphate groups were identified as critical sites for MBP-lipid interactions. Circular dichroism (CD) spectroscopy suggests that MBP adopts helical structures that penetrate the bilayer of normal MMMs. These findings offer new insights into the molecular-level interactions between MBP and myelin membranes, with implications for understanding demyelination in diseases like MS.

Keywords: model myelin membranes; myelin basic protein; van der Waals interactions; FTIR and CD spectroscopy; differential scanning calorimetry (DSC)

ugu

Academic Editor: Shiro Suetsugu

check for

updates

Received: 12 August 2025 Revised: 10 September 2025 Accepted: 15 September 2025 Published: 17 September 2025

Citation: Maleš, P.; Pem, B.; Petrov, D.; Mangiarotti, A.; Dimova, R.; Bakarić, D. Adsorption of Myelin Basic Protein on Model Myelin Membranes Reveals Weakening of van der Waals Interactions in a Lipid Ratio-Dependent Manner. *Membranes* 2025, 15, 279. https://doi.org/10.3390/membranes15090279

Copyright: © 2025 by the authors. Licensee MDPI, Basel, Switzerland. This article is an open access article distributed under the terms and conditions of the Creative Commons Attribution (CC BY) license (https://creativecommons.org/licenses/by/4.0/).

1. Introduction

Myelin is a lipid-rich extension of the plasma membrane found in oligodendrocytes within the central nervous system (CNS) and Schwann cells in the peripheral nervous system (PNS). It provides structural support and facilitates the efficient transmission of neural impulses. This efficiency is achieved through multiple layers wrapping around the axon, the dense packing of the myelin sheaths, and the very thin layer of water that exists between them [1,2]. Myelin is characterized by high lipid content, constituting 70–85%, compared to proteins, which make up 15–30% [3,4]. Major lipid classes include phospholipids (phosphatidylcholines (PCs), phosphatidylethanolamines (PEs), phosphatidylserines

(PSs), and sphingomyelin (SM)), cholesterol (CHOL), and glycosphingolipids such as galactosylcerebroside (GalC) and its sulfatide (GalC-S) form, found in an approximate molar ratio of 40%:40%:20%. The most significant proteins are proteolipid protein (PLP) and myelin basic protein (MBP); the former connects adjacent myelin layers and is a highly conserved hydrophobic protein, whereas the latter is an intrinsically disordered protein (IDP) that acts as an intramembrane adhesive element and makes up 15% of total protein content [3,5,6]. MBP exists in several isoforms, among which 18.5 kDa is the most abundant in the brains of adult humans and cattle [7–9], and the enrichment with arginine and lysine residues [10,11] makes it highly positively charged at physiological conditions [12].

A disruption of the spirally wrapped myelin sheath around the axon is referred to as demyelination. This condition encompasses effects such as unwrapping, vacuole formation, and bilayer swelling due to water and ion leakage across the sheaths [13–15]. Resulting in the impaired transmission of neural impulses, it produces clinical symptoms such as vision loss and muscle weakness, which are common features of multiple sclerosis (MS) [7,16–18]. Studies of experimental autoimmune encephalomyelitis (EAE), an animal model of MS, have demonstrated that the amount and ratios of representative myelin lipids are significantly modified compared to those in normal myelin [19]. In disordered myelin, the lipid composition was found to be significantly perturbed in favor of the increase in PE, PS and CHOL amounts with simultaneous decrease in PC and especially SM [20,21]. The adhesive ability of MBP demonstrated strong dependence on lipid composition [5,22], as well on the presence of certain cations (Ca²⁺) found in a hydrating medium [23].

Despite numerous neuroscience studies devoted to the revelation of the steps that trigger demyelination [24], the efforts that addressed demyelination at the molecular level are, to the best of our knowledge, rather scarce. Gasecka et al. demonstrated the use of Polarized Coherent Raman Microscopy (PR-CARS) to reveal that lipid order changes occur in myelin structures, even when these structures appear morphologically normal at the macroscopic scale [25]. This finding highlights the technique's ability to uncover molecular-level processes that occur during the early stages of demyelination [25]. A comprehensive study of model myelin membranes (MMMs) by small-angle X-ray scattering (SAXS) and cryo-transmission electron microscopy (cryo-TEM) demonstrated that even minor variations in lipid composition and protein content significantly affect MMM stability and induce structural changes that strikingly resemble those observed in pathological states [26]. PE-enriched MMMs, for example, undergo lamellar (L_{α})-to-inverse hexagonal ($H_{\rm II}$) phase transition at lower temperatures compared to membranes of normal composition, which is further modulated by charged solutes in the aqueous environment [27].

In addition to the previously described influence of negatively charged lipids on structuring or inducing conformational changes in MBP [28–32], Min et al. demonstrated that the altered levels of anionic lipids may deteriorate the adhesive properties of the model myelin membrane [5]. More specifically, the exceptional finding addresses the impact of the amount and ratio of anionic lipids and MBP on the loss of adhesive properties of MMMs, as well as that their swelling is not exclusively reserved for the cytoplasmic leaflet, but that it occurs on the extracellular leaflet as well [5]. To the best of our knowledge, the majority of studies undertaken so far tackle the impact of lipid mono- and bilayer composition on MBP conformation [22], whereas the impact of MBP on the organization of lipids within the bilayers, especially their phase, is scarcely studied. Thus, to address this gap, we investigated the influence of MBP on the thermotropic properties of MMMs, representing normal (healthy) and modified (disordered) myelin, highlighting the considerable increase in PS lipids in the latter [5]. Since the phase of the lipid bilayer made of the zwitterionic lipid 1,2-dipalmitoyl-sn-glycero-3-phosphocholine (DPPC) affects the secondary

Membranes 2025, 15, 279 3 of 17

structure of adsorbed MBP [33], we prepared MMMs from lipids that are in the gel phase $(L_{\beta(')})$ at room temperature and that can be converted into the fluid phase (L_{α}) by heating: DPPC, 1,2-dipalmitoyl-sn-glycero-3-phosphoethanolamine (DPPE), 1,2-dipalmitoyl-snglycero-3-phosphoserine (DPPS), brain sphingomyelin (bSM) and cholesterol (Figure 1). Although the melting temperature (T_m) , which is referred to as the peak of $L_{\beta(')} \rightarrow L_{\alpha}$ transition (i.e., the main phase transition), is not experimentally accessible for all used lipids $(T_{\rm m}$ = 41.5 °C for DPPC, 64.4 °C for DPPE, 51.4 °C for DPPS, 35–40 °C for bSM and 148 °C for CHOL [34–36]), using differential scanning calorimetry (DSC) we identified crucial differences in thermotropic properties of model myelin membranes in the presence of MBP, whereas FTIR spectroscopy data provided molecular-level insight into the impact of MBP on van der Waals forces between hydrocarbon chains in MMMs. Ultimately, we explored the dependence of the FTIR response of phosphate groups on the lipid composition and the presence of MBP, probing the hypothesis of strong interactions with positively charged amino acid residues of MBP. Molecular dynamics (MD) simulations were used to test the differences between normal and modified MMMs in terms of the strength of van der Waals interactions, whereas confocal microscopy studies explored the possible aggregation of MMMs in the presence of MBP. The results obtained clearly confirmed that the presence of MBP weakens van der Waals forces between hydrocarbon chains in MMMs in a lipid ratio-dependent manner, and, consequently, that lateral interactions between hydrocarbon chains differ for normal and modified MMMs, as well as in the presence of MBP.

Figure 1. Lipids used for preparation of MMMs: 1,2-dipalmitoyl-*sn*-glycero-3-phosphocholine (DPPC), 1,2-dipalmitoyl-*sn*-glycero-3-phosphoethanolamine (DPPE), 1,2-dipalmitoyl-*sn*-glycero-3-phosphoserine (DPPS), brain sphingomyelin (bSM) and cholesterol (CHOL).

2. Experimental

2.1. Chemicals and MMM Preparation

DPPC (Avanti, Alabaster, AL, USA, \geq 99%), DPPS (Avanti, Alabaster, AL, USA, \geq 99%), DPPE (Cayman Chemical, Ann Arbor, MI, USA, \geq 98%), bSM (Avanti, Alabaster, AL,

Membranes 2025, 15, 279 4 of 17

USA, ≥99%, porcine), CHOL (Avanti, Alabaster, AL, USA, 98%) and MBP (Sigma-Aldrich, Darmstadt, Germany, 90%, bovine) were purchased as white powders and used as received. Stock solutions of lipids in chloroform (CHCl₃; colorless liquid, Carlo Erba, Milan, Italy, p.a.) of concentration $\gamma(DPPC/DPPS/DPPE/bSM/CHOL) = 10 \text{ mg mL}^{-1}$ were prepared and further used in making the films for the preparation of multilamellar liposomes (MLVs) that mimic normal and modified MMMs in the absence and the presence of MBP. Separately, MBP was dissolved in an aqueous solution of NaCl (Kemika, Zagreb, Croatia, p.a. grade; NaCl_(aq)) of ionic strength I = 100 mM (pH ≈ 6) to achieve the mass concentration $\gamma = 0.6 \text{ mg mL}^{-1}$. After pipetting appropriate volumes of stock solutions of lipids in four flasks (two for normal MMMs and two for modified MMMs), CHCl₃ was removed from the flasks on a rotary evaporator, and the obtained films were additionally dried under an Ar stream. The films were hydrated with either an aqueous solution of $NaCl_{(aq)}$ or with an aqueous solution of NaCl_(aq) containing MBP. The hydration was followed by at least three cycles of suspension vortexing, heating up in a hot H_2O bath (up to 70 °C), and cooling in an ice bath (4 °C), where each step took 2 min. Ultimately, the mixtures with lipid molar ratios n(DPPC):n(DDPE):n(DPPS):n(bSM):n(CHOL) = 27:21:4:6:42 for normal MMMs and n(DPPC):n(DDPE):n(DPPS):n(bSM):n(CHOL) = 19:22:9:2:48 for modified MMMs were obtained. In all four samples, the mass concentration of lipids was $\gamma = 5$ mg mL⁻¹, and the molar ratio of MBP against lipids (in two of four samples) was 1:200 [37]. Lipid suspensions were used as prepared for DSC, FTIR, and confocal microscopy measurements, but were diluted up to $\gamma = 1$ mg mL⁻¹ for CD measurements and up to 0.05 mg mL⁻¹ for DLS and ELS measurements. The freshly prepared suspensions were examined in all measurements.

2.2. Dynamic and Electrophoretic Light Scattering (DLS and ELS) of LUVs: Measurements and Data Analysis

The size distribution of prepared MMMs in the absence and presence of MBP (MMM \pm MBP) was determined using dynamic light scattering (DLS) with a photon correlation spectrophotometer (Zetasizer Nano ZS, Malvern Instruments, Worcestershire, UK) that is equipped with a 532 nm green laser. The average hydrodynamic diameter (d_H) was defined as the value at the peak maximum of the volume size distribution. The reported results are the average of six measurements conducted at 25 °C. The zeta (ζ) potential was measured by electrophoretic light scattering (ELS) using a Malvern Panalytical Folded Capillary Zeta Cell. This value was calculated from the measured electrophoretic mobility according to the Henry equation, utilizing the Smoluchowski approximation. The measurements were repeated three times for accuracy. Data processing for both DLS and ELS was performed using Zetasizer software version 7.13 (Malvern Instruments) (refer to Supplementary Materials, Figure S1). All suspensions were measured at a concentration of 0.05 mg mL $^{-1}$. Knowing that MBP may exist as a monomer [38], dimer [3] or higher oligomers [31,39], in this research, the term 'MBP' designates all possible forms.

The normal and modified MMMs in the absence/presence of MBP were examined with a confocal microscope (Leica TCS-SP8, Leica Microsystems, Mannheim, Germany) equipped with a 63× water immersion objective and with OPSL-488 (Coherent, Berlin, Germany) laser (1%) in a bright field mode at room temperature. All images were stored in LAS X Life Science Microscope Software (Leica Microsystems, Mannheim, Germany, https://www.leica-microsystems.com/products/microscope-software/p/leica-las-x-ls/, accessed on 19 August 2025) and refined in the free Fiji ImageJ software package (v 2) (Figure S2).

2.3. Differential Scanning Calorimetry (DSC) of MMMs: Data Acquisition and Curve Analysis

The measurements of normal and modified MMMs in the absence/presence of MBP were conducted in the microcalorimeter Nano-DSC, TA Instruments (New Castle, DE, USA), using the TA Instruments Nano Analyze software (v 3.11.0) package. All suspensions and

Membranes **2025**, 15, 279 5 of 17

NaCl_(aq) solution were degassed for 10 min before measurements. The suspensions of lipids of normal and modified MMM \pm MBP (at lipid concentration of 5 mg mL⁻¹) were heated at a scan rate of 1 °C min⁻¹ in two repeated heating–cooling cycles in a temperature range of 10–90 °C as duplicates, whereas a reference, NaCl_(aq), was heated only once, respectively. Thermotropic properties of normal and modified MMM \pm MBP were determined from a thermal history-independent second heating run [40,41] in the following way: the DSC curve of NaCl_(aq) was subtracted from the DSC curve of MMM lipid suspensions (both obtained from the second heating run). For further analysis, a temperature range of 30–60 °C was selected, as this encompasses the main phase transition ($T_{\rm m}$) of lipid mixtures (DSC curves of individual lipids (DPPC, DPPE, DPPS, bSM and CHOL) are displayed in Figure S3, and DSC curves of MMM \pm MBP in the complete temperature range are displayed in Figure S4). After the baseline correction, $T_{\rm m}$ was determined from the maximum/maxima of the DSC curve in the examined temperature range.

2.4. FTIR Spectra of MMMs: Data Acquisition and Band Analysis

FTIR ATR spectra were measured using an INVENIO-S Bruker spectrometer equipped with a BioATR II unit and a photovoltaic LN-MCT detector, operated with OPUS 8.5 SP1 software (20200710). The KBr beamsplitter was positioned at an aperture of 1 mm, and the detector was set to a scanner velocity of 15 kHz for enhanced sensitivity in measurements. The BioATR II unit was continuously purged with N_2 gas, and its temperature was maintained using a circulating water bath controlled by a Huber Ministat 125 temperature controller. For the measurements, 20 μ L of each sample—MMM (γ (MMM) = 5 mg/mL), MBP + MMM (γ (MBP) = 0.6 mg/mL, γ (MMM) = 5 mg/mL), and NaCl_(aq)—were placed in a small circular sample compartment that utilized dual crystal technology. The FTIR spectra were recorded at temperatures of 30 °C and 60 °C to capture the FTIR spectra of MMMs in (expectedly) predominantly gel (30 °C) and fluid (60 °C) phases. Three independent measurements were conducted for each sample, except for NaCl_(aq), which was recorded once. All spectra were acquired with a nominal resolution of 2 cm $^{-1}$ and involved 256 scans.

The acquired spectra were examined in the following spectral ranges: (i) 2980–2820 cm⁻¹, which displays the bands originating from the antisymmetric (v_{as}CH₂) and symmetric (v_sCH_2) stretching of methylene groups in lipid hydrocarbon chains; (ii) 1762–1690 cm⁻¹, which contains the band originating from carbonyl stretching of the lipid glycerol backbone (ν C=O(OR)); (iii) 1485–1430 cm⁻¹, in which the scissoring (γ CH₂) of methylene groups in lipid hydrocarbon chains and the bending of the protonated amino moiety (-NH₃⁺) of MBP and DPPE appear; and (iv) 1275–1190 cm⁻¹, which reveals the band originating from the antisymmetric stretching of phosphate moieties in lipid polar headgroups ($v_{as}PO_2^-$) and of CO groups (v_{as} CO). In the selected ranges, the spectra were smoothed using the Savitzky– Golay procedure (a third-degree polynomial through 30 points), baseline-corrected (using two points at spectral minima), and normalized [42]. Additionally, we examined the region 1800–1480 cm⁻¹, which comprises, among other components, the Amide I (C=O(NH)) and Amide II (NH) bands of MBP and bSM, as well as the antisymmetric ($v_{as}COO^-$) and symmetric (v_sCOO^-) stretching of carboxylic groups of DPPS [43,44]. This spectral range is exceptionally complicated for unambiguous analysis and is displayed in the Supplementary Materials (Figure S5) but omitted from further analysis.

2.5. CD Spectra of MBP Adsorbed on MMMs: Measurements and Data Analysis

CD spectra were measured on a Jasco J-815 spectrometer in quartz cells with an optical path of 0.01 cm. 40 μL of MBP (γ (MBP) = 1.3 mg mL⁻¹, c(MBP) = 67.4 μ M), MMM (γ (MMM) = 1 mg mL⁻¹), MBP + MMM (γ (MBP) = 0.1 mg mL⁻¹; γ (MMM) = 1 mg

Membranes **2025**, 15, 279 6 of 17

mL $^{-1}$), and NaCl $_{(aq)}$ were put in quartz cells placed in temperature-controlled CD block and measured as at least two separate measurements at temperatures of 30 °C and 60 °C. The CD spectra were recorded in the wavelength range 300–190 nm with the scanning rate of 200 nm min $^{-1}$ and with 2 accumulations. Subtraction of the CD spectrum of MMMs suspended in NaCl $_{(aq)}$ in the absence of MBP from raw CD spectra of MMM + MBP was followed by their smoothing (Savitzky–Golay; polynomial of a 3rd degree and 30 points [42]). The subtracted CD spectra were analyzed using [45].

3. Results and Discussion

3.1. The Size and Aggregation of MMMs Depend on the Lipid Composition and the Presence of MBP

In the presence of MBP, the average $d_{\rm H}$ value of normal MMMs is 3–4 times larger than that of modified MMMs (Figure S1). Additionally, the size range of normal MMM + MBP is significantly broader than that of modified MMM + MBP (see Figure S1). Both phenomena are likely associated with the different interactions between MBP and normal/modified MMMs due to different lipid ratios in the latter, emphasizing the role of anionic PS lipid. Interestingly, in the absence of MBP, normal and modified MMMs are of comparable diameter. ζ -potential approaches zero in the presence of positively charged MBP, although this effect is more pronounced in normal MMMs than in modified MMMs owing to the different amount of anionic lipid (Figure S1). Confocal microscopy provided further evidence of protein-driven effects. Imaging showed clear aggregation of MMMs in the presence of MBP, consistent with earlier reports describing MBP's ability to promote vesicle clustering and membrane adhesion [11,46,47] (Figure S2). These findings support the idea that MBP not only alters the average vesicle size but also drives their aggregation through primarily electrostatic interactions.

3.2. MBP Modulates Thermotropic Properties of Normal and Modified MMMs in a Qualitatively Different Manner

In the context of thermotropic properties of lipid membranes, the most distinguished one is the main phase transition or melting, i.e., the transition of lipid bilayers from the gel ($L_{\beta(')}$) to fluid (L_{α}) phase. The main phase transition has a peak at the melting temperature (T_m), and comprehensive calorimetric studies, subsequently supported by microscopic studies, revealed that the length and (un)saturation degree of hydrocarbon chains of lipid molecules are determining factors in the magnitude of T_m values [36,48]. More specifically, the main phase transition of lipid bilayers primarily involves reduced van der Waals interactions among hydrocarbon chains, increased hydration of the polar headgroup region, and subsequent thinning of the bilayer [49–53].

The crucial difference between normal MMMs in the presence and absence of MBP is that in the former there are no thermotropic events in the temperature range 30–60 °C, whereas in the latter, two unresolved maxima appear at 41.4 \pm 0.1 °C and 44.3 \pm 0.1 °C (Figure 2). On the contrary, in modified MMMs in the presence of MBP, DSC curve displays three maxima at 35.5 \pm 0.1 °C, 39.8 \pm 0.1 °C and 45.4 \pm 0.1 °C, while in its absence only one at 39.4 \pm 0.1 °C. By comparing these values with those of individual lipids (see Figures S3 and S4), it seems reasonable to assume that the melting of bSM and of DPPC is the dominant process. Moreover, the emergence of multiple transitions implies a more heterogeneous lipid organization in the presence of MBP.

However, what is rather peculiar is that MBP, depending on the lipid composition, may suppress some physicochemical features; in particular, in normal MMMs in the presence MBP, van der Waals forces are reduced even at 30 $^{\circ}$ C, i.e., when individual lipids are predominantly in the gel phase. This further implies that the interaction of MBP with the

Membranes 2025, 15, 279 7 of 17

lipid membrane surface highly depends on the lipid composition (normal vs. modified) and likely on their distribution. A possible explanation for this is that either MBP in some fashion penetrates the bilayer and interferes with the lipid packing pattern through a direct interaction between particular functional groups or simply that it drastically changes the hydration level of surrounding lipid molecules, which ultimately causes weakening of the van der Waals interactions. These two possibilities are further explored by FTIR and CD spectra of MMM \pm MBP systems.

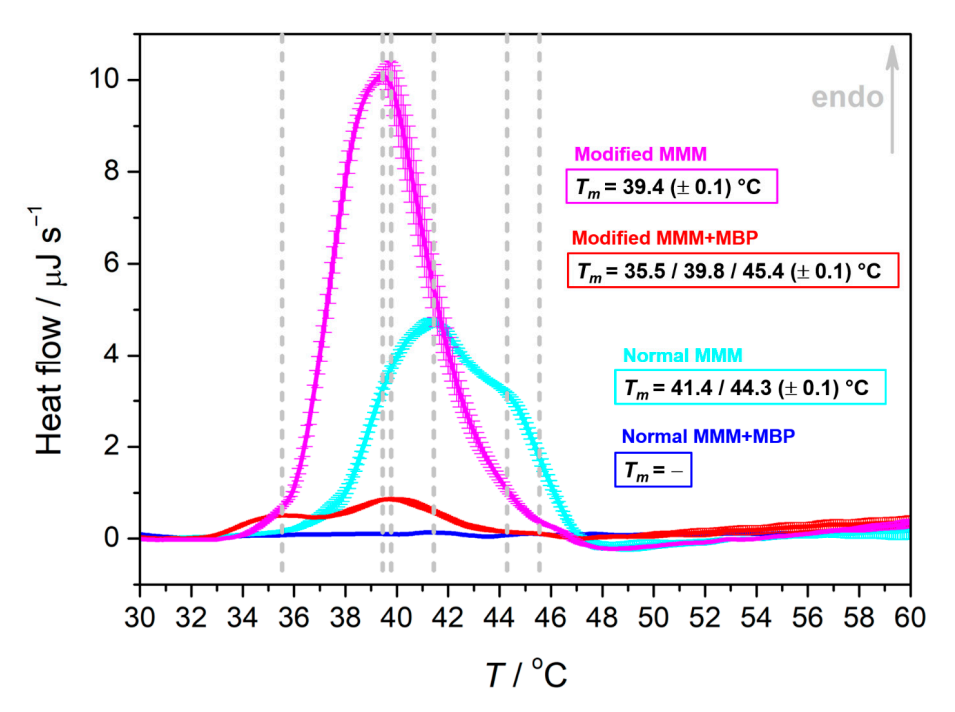


Figure 2. DSC curves of MMM systems in the absence/presence of MBP (blue curve: normal MMM + MBP, cyan curve: normal MMMs; red curve: modified MMM + MBP; magenta curve: modified MMMs) obtained as an average of two measurements with associated uncertainties. Phase transition temperatures are highlighted with dashed lines and are additionally written on graphs and designated with a corresponding color.

3.3. MBP-Induced Weakening of van der Waals Interactions Between Hydrocarbon Chains Depends on Lipid Composition

The first examined spectral region (2980–2820 cm⁻¹) shows the bands that arise from the (anti)symmetric stretching of CH₂ groups of hydrocarbon chains (Figure 3a). Regardless of the kind of lipids (in terms of their polar headgroups), the band maxima usually experience a high-frequency shift for about 4 cm⁻¹ upon the transformation of the lipids from the gel to fluid phase [54–58], i.e., the weakening of van der Waals interactions [41,59,60]. In this research, an extraordinary phenomenon is detected; for normal MMMs in the presence of MBP the band maximum originated from $v_{as}CH_2$ upon heating undergoes a low-frequency shift, i.e., from 2924 cm⁻¹ (at 30 °C) to 2921 cm⁻¹ (at 60 °C), whereas v_sCH_2 maintains the position of the band maximum at both temperatures (at 2852 cm⁻¹ at 30 °C and 60 °C). Contrary to the expected high-frequency shift of both band maxima, this phenomenon implies that upon heating, van der Waals forces between lipid hydrocarbon chains are weaker at 30 °C than at 60 °C. This finding is in line with thermotropic properties (Figure 2) of the normal MMM + MBP system, since the DSC curve does not capture the melting process. Interestingly, in normal MMMs, a similar response is observed; the $v_{as}CH_2$ band maximum undergoes a low-frequency shift, i.e., from 2924 cm⁻¹ (at 30 °C) to 2922 cm^{-1} (at $60 \,^{\circ}\text{C}$), and $v_s\text{CH}_2$ band maximum remains at the same place at both temperatures (at 2853 cm⁻¹ at 30 °C and 60 °C). Although it could be deduced that mere

Membranes **2025**, 15, 279 8 of 17

composition of MMMs is the decisive factor for the strength of van der Waals interactions, we would like to draw attention to the DSC curve of normal MMMs. As seen in Figure 2, normal MMMs in the absence of MBP displays the main phase transition, suggesting that the heating weakens van der Waals interaction between hydrocarbon chains, i.e., that they are preserved in the gel phase. Thus, it appears that the factor(s) other than just lipid composition play(s) a role in the appearance of FTIR spectra in this spectral region, which also agrees with the DSC response (more details are elaborated in subsequent subsections). Unlike normal MMM \pm MBP, modified MMM \pm MBP displays the expected high-frequency shift upon gel-to-fluid phase transition: in the presence of MBP they are displaced of from ν_{as} CH₂ band from 2924 cm $^{-1}$ (at 30 °C) to 2926 cm $^{-1}$ (at 60 °C), while in the absence of MBP from 2922 cm $^{-1}$ (at 30 °C) to 2925 cm $^{-1}$ (at 60 °C), respectively. The maximum of the band originating from ν_{s} CH₂ maintains the position at 2852 cm $^{-1}$ in both gel and fluid phase (at 30 °C and at 60 °C).

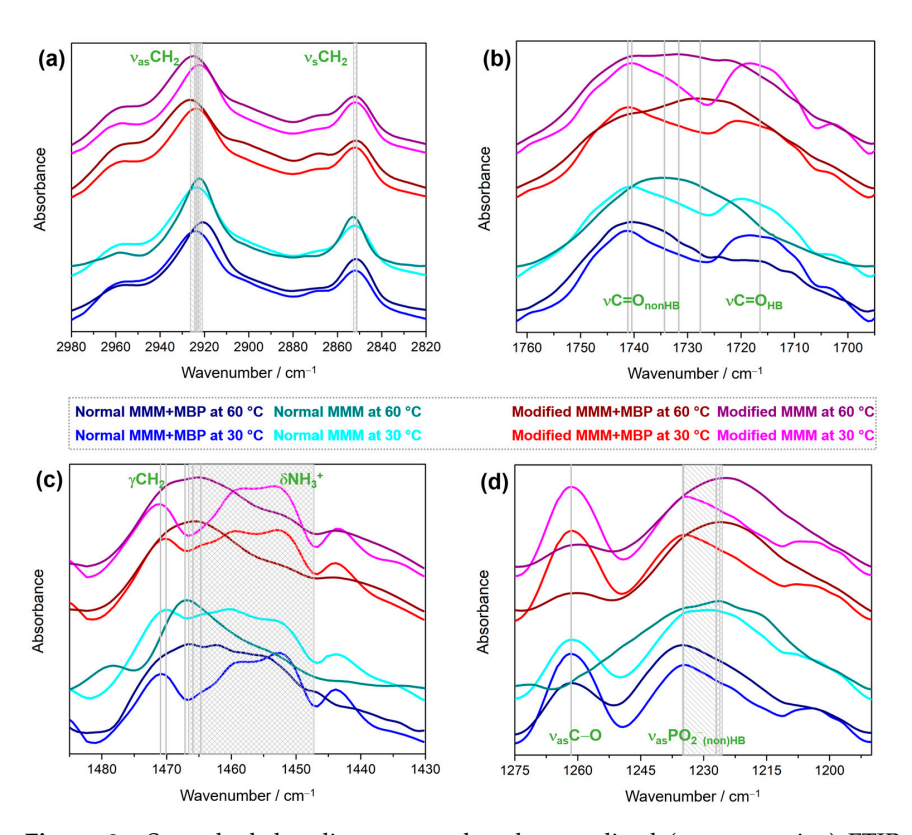


Figure 3. Smoothed, baseline-corrected and normalized (representative) FTIR spectra of normal and modified MMM \pm MBP collected at 30 °C and 60 °C in the following spectral regions: (a) 2980–2820 cm $^{-1}$ ($\nu_{as}CH_2$ and ν_{s} CH $_2$); (b) 1765–1690 cm $^{-1}$ ($\nu_{C}=O_{(non)HB}$); (c) 1485–1430 cm $^{-1}$ ($\gamma_{C}CH_2$ and $\delta_{C}NH_3^+$); (d) 1275–1190 cm $^{-1}$ ($\nu_{as}C-O$, $\nu_{as}PO_2^-$ ($\nu_{an}N_{BB}$). The spectra were designated as follows: normal MMM + MBP with blue (30 °C) and navy (60 °C), normal MMMs with cyan (30 °C) and dark cyan (60 °C), modified MMM + MBP with red (30 °C) and wine (60 °C), modified MMMs with purple (30 °C) and magenta (60 °C). Note: We would like to draw the reader's attention to the legend in the middle of the image.

The second spectral region (1762–1690 cm $^{-1}$) reveals the bands originating from the stretching of the carbonyl moiety of the glycerol backbone, which can be either free from hydrogen bonding with water molecules from the interfacial layer (ν C=O_{nonHB}) or involved in a hydrogen bonding (ν C=O_{HB}) (Figure 3b) [61]. In both normal and modified MMM systems at 30 °C, regardless of the MBP, the spectral envelopes are qualitatively rather similar: in normal MMM + MBP/normal MMMs the maxima assigned as ν C=O_{nonHB} and ν C=O_{HB} appear at 1741 cm $^{-1}$ /1744 cm $^{-1}$ and 1718 cm $^{-1}$ /1716 cm $^{-1}$, whereas in

Membranes 2025, 15, 279 9 of 17

modified MMM + MBP/normal MMMs the maxima assigned as ν C=O_{nonHB} and ν C=O_{HB} appear at 1741 cm⁻¹/1740 cm⁻¹ and 1721 cm⁻¹/1718 cm⁻¹, respectively. On the other hand, the spectra at 60 °C display differences attributed to the larger number of maxima in the region in which ν C=O_{HB} absorbs (Figure 3b). In particular, in normal MMM + MBP system the maxima assigned as ν C=O_{nonHB} are detected at 1741 cm⁻¹, and the ν C=O_{HB} at 1724 cm⁻¹, 1717 cm⁻¹, and 1710 cm⁻¹. In normal MMMs, the maximum at 1735 cm⁻¹ is a result of a superposition of ν C=O_{nonHB} and ν C=O_{HB} bands. In modified MMM + MBP, the corresponding maxima appear at 1741 cm⁻¹ and 1728 cm⁻¹, whereas in modified MMMs the maxima are seen at 1740 cm⁻¹, 1734 cm⁻¹, 1731 cm⁻¹, and at 1723 cm⁻¹. The absence of a certain trend in the position and number of band maxima observed in this spectral region suggests that the hydration of the glycerol moiety is a rather delicate function of the amount of bSM [62], as well as on their interaction with CHOL [63–65].

As seen from the third spectral region $(1485-1430 \text{ cm}^{-1})$; Figure 3c), the lateral packing of hydrocarbon chains distinguishes depending on both MMM lipid composition and the presence of MBP: at 30 $^{\circ}$ C in normal MMM + MBP the band maximum at 1471 cm⁻¹ implies that van der Waals forces between hydrocarbon chains are rather weak [55,66], which is opposite for normal MMM system in which the maximum at 1467 cm⁻¹ suggest higher order in the packing pattern (more gel-like). The analogous signals in modified MMM + MBP and modified MMMs appear at 1470 cm⁻¹ and at 1471 cm⁻¹, respectively, suggesting a disorder level comparable to that in normal MMM + MBP. Interestingly, at 60 °C the corresponding band maximum appears at 1467 cm⁻¹ (normal MMM + MBP), at 1470 cm^{-1} (normal MMMs), at 1466 cm^{-1} (modified MMM + MBP), and at 1465 cm^{-1} (modified MMMs). The comparison of the values shown by normal MMM + MBP are in line with the data detected in the first examined spectral regions, that van der Waals forces between hydrocarbon chains are weaker at 30 °C than at 60 °C. For normal MMMs, the conclusion drawn from this spectral region is in line with DSC data, which suggests expectedly weaker van der Waals interactions between hydrocarbon chains at 60 $^{\circ}\text{C}$ than at 30 °C [55,66]. The displacement of the wavenumber maxima in the first spectral region of normal MMMs remains, unfortunately, unexplained. Tentatively, the amount of bSM and interdigitation of hydrocarbon chains in normal MMMs may contribute to the observed phenomenon [67–69], irrespective to the MBP, but the presence of MBP unambiguously modulates van der Waals interactions between hydrocarbon chains and consequently affects their fluidity at 30 °C and 60 °C. The position of the band maxima at 60 °C in modified MMMs is compromised by the superposition with the bands originating from the bending of -NH₃⁺ moieties of DPPE and DPPS lipids, as well as of lysine (Lys) residues of MBP [33]. In general, these signals in modified MMM \pm MBP systems resemble each other at the corresponding temperature, whereas in normal MMM \pm MBP they vary with the presence of MBP and the phase. As previously reported, Lys-originated bands are highly sensitive to the phase of lipid bilayers, while owing to their positive charge, their response is modulated by the amount of anionic lipids [11,16,70,71], among which PS lipids are considerably higher in modified than in normal MMMs [5,70,72].

Besides containing the band originating from the antisymmetric stretching of C–O moiety (ν_{as} C–O), the fourth spectral region (1275–1190 cm⁻¹) reveals the envelope resulting from the antisymmetric stretching of phosphate groups that are both non-hydrogen-bonded and hydrogen-bonded (ν_{as} PO₂ $^-$ (non)HB) (Figure 3d). The former band maximum expectedly appears at 1261–1262 cm⁻¹ at 30 °C/1260–1262 cm⁻¹ at 60 °C, whereas the latter displays rather different temperature/phase-dependent features depending on the MMM composition and the presence of MBP. In normal MMM \pm MBP systems, the position of the envelope maximum barely displaces upon the phase change, remaining at 1235 cm⁻¹ after heating, while in normal MMMs it exhibits a small low-frequency shift (from 1228 cm⁻¹

to 1226 cm $^{-1}$). A change in the envelope appearance at the low-frequency side suggests that the hydration of phosphate groups of lipid molecules at 60 °C in normal MMMs is not only different from that in normal MMM + MBP, but also more heterogeneous (several maxima are seen). At this stage, it seems reasonable to conclude that the adsorption of MBP onto normal MMMs and the interaction of positively charged residues with phosphate groups attenuate the hydration of phosphate groups. On the contrary, in modified MMM \pm MBP systems, the envelopes qualitatively resemble each other and also exhibit a considerable phase transition-induced low-frequency shift in the envelope maximum; in modified MMM + MBP, the maximum displaces from 1234 cm $^{-1}$ (30 °C) to 1226 cm $^{-1}$ (60 °C), whereas in modified MMMs from 1234 cm $^{-1}$ (30 °C) to 1225 cm $^{-1}$ (60 °C). Overall, it seems straightforward to conclude that the hydration of phosphate groups in normal and modified MMMs is a function of the total lipid charge and distribution, and that the presence of MBP, depending on the composition of MMMs (normal vs. modified), may additionally perturb the hydration pattern by engaging electrostatically with headgroups.

Owing to the obscurity of Amide I/II bands by the signals emerged from bSM (and CHOL) [73] (see Figures S5 and S6), the unambiguous analysis from linear FTIR spectra [74,75] of was prevented so they are not included in the data analysis and interpretation.

3.4. Secondary Structure of MBP Depends on MMM Composition and the Phase

Following the CD spectra of MBP adsorbed on normal and modified MMMs (Figure 4), it is clear that only the normal MMM at 30 °C presents the expected CD spectrum of an intrinsically disordered protein such as MBP (blue curve with maximum at about 190 nm). Upon heating, the spectrum becomes positive, suggesting the presence of helical structures (navy curve). In modified MMMs, regardless of the global phase of lipids, the spectra resemble one another (red and wine curves). The maxima/minima at about 208 nm and 220 nm suggest that MBP in the modified MMM system is not as disordered as in a normal MMM system, and there is a certain amount of alpha-helical structures [32,76]. Considering that the BestSel [45] reported the presence of helical structures for normal MMM + MBP at 60 °C only (Figure S7), despite of large uncertainties, it seems more likely that MBP forms a differently disordered structure when adsorbed onto normal MMMs than onto modified MMMs. When elaborating the structuring of MBP, an important issue that emerges from the conducted experiments is the temperature range in which the systems were prepared, i.e., the expected gel-to-fluid phase transition of the used lipids requires temperatures higher than physiological ones. As the heating makes IDPs transformation from one distribution of secondary structures to another one [77,78], we expect that temperatures as high at $60\ ^{\circ}\text{C}$ will not decompose MBP. Moreover, in comparison with CD spectra of MBP dissolved in aqueous medium, where it displays only the signal at 195 nm (see Figure S8, data taken from [33]), MBP adsorbed onto MMMs only changes the distribution of secondary structures, which, according to Figure 4 (and Figure S7), depends on the MMM composition. In turn, this means that the lipid composition is a primary, and the lipid bilayer phase is a secondary factor in dictating MBP secondary structure [11,16,31,33,71].

3.5. Implications of MBP Adsorption on the Changes in Lipid Membrane Fluidity and Aggregation

Since the adsorption of MBP on normal MMMs clearly weakens van der Waals interactions between hydrocarbon chains at 30 $^{\circ}$ C and then slightly increases them at 60 $^{\circ}$ C (but maintaining the fluid phase), the finding emerging from this phenomenon directly tackles the variability in the bilayer fluidity. Other researchers have already recognized the importance of this issue. For instance, when exploring myelin-like monolayers that mimic the cytoplasmic leaflet that exclusively contains PS lipids, Widder et al. found that

Membranes 2025, 15, 279 11 of 17

electrostatic interactions between negatively charged PS-containing monolayers and MBP lowered the fluidity of myelin-like monolayers [20], but also that the amount of bSM may be critical for maintaining fluidity [16]. More specifically, bSM introduces complexity to the organization of lipid bilayer phases due to the asymmetry of the hydrocarbon chains (Figure 1) and the accompanying interdigitation [79]. Using structural and microscopic techniques, Krugmann et al. revealed that the interaction of MBP with lipids in myelin varies with the composition, which may increase their instability and enhance local curvature [80]. In particular, they found that the diseased myelin has lower bending rigidity and experiences high local curvature [81], which was also potentially associated with variable bSM content [80].

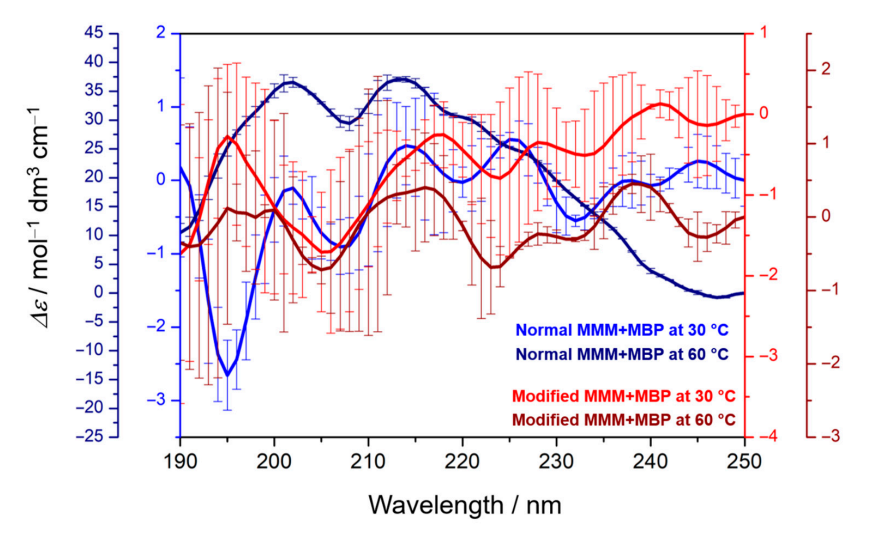


Figure 4. CD spectra of: normal MMM + MBP at $30 \,^{\circ}\text{C}/60 \,^{\circ}\text{C}$ (blue/navy); modified MMM + MBP at $30 \,^{\circ}\text{C}/60 \,^{\circ}\text{C}$ (red/wine).

Nevertheless, when CD data are compared along with DSC and FTIR results, especially for normal MMMs in the presence of MBP at 60 $^{\circ}$ C, it suggests that a certain fraction of helical structures of MBP may be formed upon interactions with lipid membranes. A certain part of MBP may penetrate the bilayers, causing overall stiffening of the normal MMM (lower band maximum at 60 $^{\circ}$ C than at 30 $^{\circ}$ C) [30]. At both temperatures, the van der Waals interactions are clearly weaker in normal than in modified MMMs, but MBP potentially inserts into the membrane, making overall packing more compact than mere normal MMMs.

MD simulations of the normal and modified systems were, unfortunately, only feasible in the absence of MBP. MBP, as an intrinsically disordered protein, does not have a well-defined initial conformation, and due to the known sampling limitations of MD (difficulties in achieving convergence), any membrane interaction will be heavily biased by the initial setup. Since adequate exploration of MBP conformational space would require separate enhanced sampling simulations and the usage of different force fields, it was declared to be out of the scope of this study [82–84]. The simulations of MMMs alone, especially the results addressed to the maintenance of van der Waals interactions at 30 $^{\circ}$ C and 60 $^{\circ}$ C) are presented in Supplementary Materials (Section S5).

In the context of the impact of MBP on lipid-dependent MMM fluidity, the results provided from the reported studies may be in line with our observation as well. However, some important differences should be highlighted. The MBP-induced aggregation appears to be a critical factor in the development not only of MS [38], but also of other pathological states [85–87]. In particular, the aggregation of lipid bilayers in the presence of MBP is expected to be the function of lipid ratio [11], but our microscopic experiments were not

able to elucidate the differences between the aggregation of normal and modified MMMs in the presence of MBP. A potential cause for the lack of information in this context may arise from the size of lipid bilayers since we worked with MLVs as MMMs, whereas Mac Millan et al. used large unilamellar vesicles (LUVs) [11]. Finally, besides the fact that some authors highlight the importance of certain lipids like bSM for mono- or bilayer fluidity [38], it seems reasonable to assume that the altered amount of CHOL also contributes to the modulation of van der Waals forces and overall bilayer fluidity [88,89]. Owing to the complexity of this research, these results will be presented in a subsequent study.

4. Conclusions

By building up the MMMs from the same lipids, but at different ratios, we revealed that van der Waals forces between hydrocarbon chains are considerably weaker for the lipid composition that mimics normal myelin as opposed to that of modified myelin. DSC study confirmed the absence of any thermotropic event in normal MMMs in the presence of MBP, whereas FTIR spectra suggest that for normal MMM \pm MBP van der Waals interactions are substantially weak at both 30 °C and 60 °C (from the bands originating from antisymmetric stretching of methylene groups). However, for normal MMMs in the presence of MBP, the additional confirmation of van der Waals forces weakness at both temperatures emerges from the signal originating from scissoring of methylene groups that indicate no change in the lateral arrangement between lipid molecules at both temperatures. Moreover, the hydration of phosphate groups of lipids in normal MMMs is substantially different from that in modified MMMs. In the context of CD measurements, it is suggested that MBP has a different disordered structure when adsorbed at the surface of normal and modified MMMs. Owing to the possibility of displaying a certain amount of helical structure in normal MMMs at 60 °C, its hydrophobic parts may insert into the bilayer and stiffen it, which coincides with heating-induced displacement of the maximum of antisymmetric stretching of methylene groups. To the best of our knowledge, this manuscript is the first example that highlights the molecular-level insight into the lipid ratio-dependent weakening of van der Waals interactions between hydrocarbon chains that directly impacts the fluidity and tackles aggregation-induced effects that emerge upon the adsorption of IDP.

Supplementary Materials: The following supporting information can be downloaded at: https: //www.mdpi.com/article/10.3390/membranes15090279/s1, Figure S1: The size and ζ -potential data of normal and modified MMM and the absence and presence of MBP obtained at 25 °C; Figure S2: Confocal microscope images of MMM in bright field (scale bars: 2 and 20 µm as indicated on the images): (a) normal MMM + MBP; (b) modified MMM + MBP; (c) normal MMM; (d) modified MMM; Figure S3. DSC curves of individual lipids with highlighted phase transition(s) temperature(s) (DPPC-red; DPPS-blue; DPPE-green, bSM-cyan; CHOL-gray); Figure S4. DSC curves of normal and modified MMM in the absence and presence of MBP (normal and modified MMM \pm MBP) in the 10–90 °C temperature range; Figure S5. FTIR spectra of normal and modified MMM in the absence and presence of MBP (normal and modified MMM \pm MBP) in the spectral range 1800–1480 cm⁻¹ acquired at 30 °C and 60 °C (the legend is displayed on the right side of the figure); Figure S6. FTIR spectra of bSM (a) and MBP (b) in the spectral range 1800–1480 cm⁻¹ acquired at 20 °C and 50 °C; Figure S7. Fractions of secondary structures in normal and modified MMM in the absence and presence of MBP (normal and modified MMM \pm MBP) obtained from BestSel; Experimental CD spectra of MBP dissolved in NaCl_(aq) at 20 °C and 50 °C; Figure S9. Deuterium order parameters (-S_{CD}) of palmitic acid chains within lipids in normal and modified MMM, at 30 °C and 60 °C; Figure S10. Final snapshots of the simulated systems, with a representative lipid of each type (DPPC—blue, DPPE—orange, DPPS—green, SSM—purple, CHOL—black) highlighted: top left—normal MMM at 30 °C, top right—modified MMM at 30 °C,

bottom left—normal MMM at $60\,^{\circ}$ C, bottom right—modified MMM at $60\,^{\circ}$ C; Table S1: Structural parameters of model membranes: area per lipid (APL), membrane thickness (MT) and lateral diffusion coefficient (D).

Author Contributions: Conceptualization, D.B.; methodology, D.B.; software, B.P. and D.P.; validation, D.B. and R.D.; formal analysis, B.P. and D.B.; investigation, P.M. and A.M.; resources, D.B. and R.D.; data curation, B.P. and D.B.; writing—original draft preparation, D.B., B.P. and R.D.; writing—review and editing, D.B., B.P. and D.P.; visualization, B.P. and D.P.; supervision, D.B.; project administration, D.B.; funding acquisition, D.B. and R.D. All authors have read and agreed to the published version of the manuscript.

Funding: This research was funded by the Croatian Science Foundation, Project No. UIP-2020-02-7669 (led by D.B.) and by a bilateral project "Myelin protein impact on membrane phase state, morphology and structure (ImProMem)" financed by the Croatian Ministry of Science and Education (MSE) (led by D.B.) and the German Academic Exchange Service (Deutscher Akademischer Austauschdienst, DAAD) (led by R.D.).

Institutional Review Board Statement: Not applicable.

Data Availability Statement: The original contributions presented in this study are included in the article/Supplementary Material. Further inquiries can be directed to the corresponding author.

Acknowledgments: We sincerely thank the members of the Laboratory for biocolloids and surface chemistry (Division for Physical Chemistry, Ruđer Bošković Institute) for enabling access to the Zetasizer Nano ZS (Malvern).

Conflicts of Interest: The authors declare no conflict of interest.

References

- Caprariello, A.V.; Rogers, J.A.; Morgan, M.L.; Hoghooghi, V.; Plemel, J.R.; Koebel, A.; Tsutsui, S.; Dunn, J.F.; Kotra, L.P.; Ousman, S.S.; et al. Biochemically Altered Myelin Triggers Autoimmune Demyelination. *Proc. Natl. Acad. Sci. USA* 2018, 115, 5528–5533. [CrossRef]
- 2. Snaidero, N.; Simons, M. Myelination at a Glance. J. Cell Sci. 2014, 127, 2999–3004. [CrossRef] [PubMed]
- 3. Quarles, R.H. *Myelin Lipids and Proteins: Structure, Function, and Roles in Neurological Disorders*; Sibley, D.R., Hanin, I., Kuhar, M., Skolnick, P., Eds.; John Wiley & Sons, Ltd.: Hoboken, NJ, USA, 2007.
- 4. Poitelon, Y.; Kopec, A.M.; Belin, S. Myelin Fat Facts: An Overview of Lipids and Fatty Acid Metabolism. *Cells* **2020**, *9*, 812. [CrossRef] [PubMed]
- 5. Min, Y.; Kristiansen, K.; Boggs, J.M.; Husted, C.; Zasadzinski, J.A.; Israelachvili, J. Interaction Forces and Adhesion of Supported Myelin Lipid Bilayers Modulated by Myelin Basic Protein. *Proc. Natl. Acad. Sci. USA* **2009**, *106*, 3154–3159. [CrossRef]
- 6. Palavicini, J.P.; Wang, C.; Chen, L.; Ahmar, S.; Higuera, J.D.; Dupree, J.L.; Han, X. Novel Molecular Insights into the Critical Role of Sulfatide in Myelin Maintenance/Function. *J. Neurochem.* **2016**, *139*, 40–54. [CrossRef]
- 7. Träger, J.; Meister, A.; Hause, G.; Harauz, G.; Hinderberger, D. Shaping Membrane Interfaces in Lipid Vesicles Mimicking the Cytoplasmic Leaflet of Myelin through Variation of Cholesterol and Myelin Basic Protein Contents. *Biochim. Biophys. Acta Biomembr.* 2023, 1865, 184179. [CrossRef] [PubMed]
- 8. Raasakka, A.; Kursula, P. Flexible Players within the Sheaths: The Intrinsically Disordered Proteins of Myelin in Health and Disease. *Cells* **2020**, *9*, 470. [CrossRef]
- 9. Harauz, G.; Ishiyama, N.; Hill, C.M.D.; Bates, I.R.; Libich, D.S.; Farès, C. Myelin Basic Protein—Diverse Conformational States of an Intrinsically Unstructured Protein and Its Roles in Myelin Assembly and Multiple Sclerosis. *Micron* **2004**, *35*, 503–542. [CrossRef]
- 10. Beniac, D.R.; Luckevich, M.D.; Czarnota, G.J.; Tompkins, T.A.; Ridsdale, R.A.; Ottensmeyer, F.P.; Moscarello, M.A.; Harauz, G. Three-Dimensional Structure of Myelin Basic Protein: I. Reconstruction via Angular Reconstitution of Randomly Oriented Single Particles. *J. Biol. Chem.* 1997, 272, 4261–4268. [CrossRef]
- 11. Mac Millan, S.V.; Ishiyama, N.; White, G.F.; Palaniyar, N.; Hallett, F.R.; Harauz, G. Myelin Basic Protein Component C1 in Increasing Concentrations Can Elicit Fusion, Aggregation, and Fragmentation of Myelin-like Membranes. *Eur. J. Cell Biol.* **2000**, 79, 327–335. [CrossRef]
- 12. Harauz, G.; Boggs, J.M. Myelin Management by the 18.5-kKDa and 21.5-kDa Classic Myelin Basic Protein Isoforms. *J. Neurochem.* **2013**, 125, 334–361. [CrossRef]

13. Mahajan, K.R.; Herman, D.; Zheng, Y.; Androjna, C.; Thoomukuntla, B.; Ontaneda, D.; Nakamura, K.; Trapp, B.D. Neurodegeneration and Demyelination in the Multiple Sclerosis Spinal Cord: Clinical, Pathological, and 7T MRI Perspectives. *Neurology* **2025**, 104, e210259. [CrossRef]

- 14. Osorio-Querejeta, I.; Sáenz-Cuesta, M.; Muñoz-Culla, M.; Otaegui, D. Models for Studying Myelination, Demyelination and Remyelination. *Neuromol. Med.* **2017**, *19*, 181–192. [CrossRef]
- 15. Osorio-Querejeta, I.; Alberro, A.; Muñoz-Culla, M.; Mäger, I.; Otaegui, D. Therapeutic Potential of Extracellular Vesicles for Demyelinating Diseases; Challenges and Opportunities. *Front. Mol. Neurosci.* **2018**, *11*, 434. [CrossRef]
- 16. Widder, K.; Harauz, G.; Hinderberger, D. Myelin Basic Protein (MBP) Charge Variants Show Different Sphingomyelin-Mediated Interactions with Myelin-like Lipid Monolayers. *Biochim. Biophys. Acta Biomembr.* **2020**, *1862*, 183077. [CrossRef]
- 17. Desai, R.A.; Davies, A.L.; Tachrount, M.; Kasti, M.; Laulund, F.; Golay, X.; Smith, K.J. Cause and Prevention of Demyelination in a Model Multiple Sclerosis Lesion. *Ann. Neurol.* **2016**, *79*, 591–604. [CrossRef]
- 18. Rodriguez, M. Effectors of Demyelination and Remyelination in the CNS: Implications for Multiple Sclerosis. *Brain Pathol.* **2007**, 17, 219–229. [CrossRef] [PubMed]
- 19. Schmidt, T.; Situ, A.J.; Ulmer, T.S. Structural and Thermodynamic Basis of Proline-Induced Transmembrane Complex Stabilization. *Sci. Rep.* **2016**, *6*, 29809. [CrossRef] [PubMed]
- 20. Widder, K.; Träger, J.; Kerth, A.; Harauz, G.; Hinderberger, D. Interaction of Myelin Basic Protein with Myelin-like Lipid Monolayers at Air-Water Interface. *Langmuir* **2018**, 34, 6095–6108. [CrossRef] [PubMed]
- 21. Olsen, A.S.B.; Færgeman, N.J. Sphingolipids: Membrane Microdomains in Brain Development, Function and Neurological Diseases. *Open Biol.* **2017**, *7*, 170069. [CrossRef]
- Lee, D.W.; Banquy, X.; Kristiansen, K.; Kaufman, Y.; Boggs, J.M.; Israelachvili, J.N. Lipid Domains Control Myelin Basic Protein Adsorption and Membrane Interactions between Model Myelin Lipid Bilayers. *Proc. Natl. Acad. Sci. USA* 2014, 111, E768–E775.
 [CrossRef]
- 23. Weil, M.T.; Möbius, W.; Winkler, A.; Ruhwedel, T.; Wrzos, C.; Romanelli, E.; Bennett, J.L.; Enz, L.; Goebels, N.; Nave, K.A.; et al. Loss of Myelin Basic Protein Function Triggers Myelin Breakdown in Models of Demyelinating Diseases. *Cell Rep.* **2016**, *16*, 314–322. [CrossRef]
- 24. Don, A.S.; Hsiao, J.H.T.; Bleasel, J.M.; Couttas, T.A.; Halliday, G.M.; Kim, W.S. Altered Lipid Levels Provide Evidence for Myelin Dysfunction in Multiple System Atrophy. *Acta Neuropathol. Commun.* **2014**, *2*, 150. [CrossRef] [PubMed]
- Gasecka, P.; Jaouen, A.; Bioud, F.Z.; de Aguiar, H.B.; Duboisset, J.; Ferrand, P.; Rigneault, H.; Balla, N.K.; Debarbieux, F.; Brasselet, S. Lipid Order Degradation in Autoimmune Demyelination Probed by Polarized Coherent Raman Microscopy. *Biophys. J.* 2017, 113, 1520–1530. [CrossRef]
- 26. Shaharabani, R.; Ram-On, M.; Avinery, R.; Aharoni, R.; Arnon, R.; Talmon, Y.; Beck, R. Structural Transition in Myelin Membrane as Initiator of Multiple Sclerosis. *J. Am. Chem. Soc.* **2016**, *138*, 12159–12165. [CrossRef]
- 27. Shaharabani, R.; Ram-On, M.; Talmon, Y.; Beck, R. Pathological Transitions in Myelin Membranes Driven by Environmental and Multiple Sclerosis Conditions. *Proc. Natl. Acad. Sci. USA* **2018**, *115*, 11156–11161. [CrossRef]
- 28. Raasakka, A.; Ruskamo, S.; Kowal, J.; Barker, R.; Baumann, A.; Martel, A.; Tuusa, J.; Myllykoski, M.; Bürck, J.; Ulrich, A.S.; et al. Membrane Association Landscape of Myelin Basic Protein Portrays Formation of the Myelin Major Dense Line. *Sci. Rep.* **2017**, 7, 4974. [CrossRef] [PubMed]
- 29. Raasakka, A.; Jones, N.C.; Hoffmann, S.V.; Kursula, P. Ionic Strength and Calcium Regulate Membrane Interactions of Myelin Basic Protein and the Cytoplasmic Domain of Myelin Protein Zero. *Biochem. Biophys. Res. Commun.* **2019**, *511*, 7–12. [CrossRef]
- Keniry, M.A.; Smith, R. Circular dichroic analysis of the secondary structure of myelin basic protein and derived peptides bound to detergents and to lipid vesicles. *Biochim. Biophys. Acta* 1979, 578, 381–391. [CrossRef] [PubMed]
- 31. Smith, R. The Basic Protein of CNS Myelin: Its Structure and Ligand Binding. J. Neurochem. 1992, 59, 1589–1608. [CrossRef]
- 32. Polverini, E.; Fasano, A.; Zito, F.; Riccio, P.; Cavatorta, P. Conformation of Bovine Myelin Basic Protein Purified with Bound Lipids. *Eur. Biophys. J.* 1999, *28*, 351–355. [CrossRef]
- 33. Maleš, P.; Brkljača, Z.; Crnolatac, I.; Petrov, D.; Bakarić, D. Phase-Dependent Adsorption of Myelin Basic Protein to Phosphatidyl-choline Lipid Bilayers. *Membranes* **2024**, *14*, 15. [CrossRef]
- 34. Koynova, R.; Caffrey, M. Phases and Phase Transitions of the Phosphatidylcholines. *Biochim. Biophys. Acta Rev. Biomembr.* **1998**, 1376, 91–145. [CrossRef]
- 35. Koynova, R.; Caffrey, M. Phases and Phase Transitions of the Sphingolipids. Biochim. Biophys. Acta 1995, 1255, 213–236. [CrossRef]
- 36. Marsh, D. Structural and Thermodynamic Determinants of Chain-Melting Transition Temperatures for Phospholipid and Glycolipids Membranes. *Biochim. Biophys. Acta Biomembr.* **2010**, *1798*, 40–51. [CrossRef]
- 37. Schmitt, S.; Castelvetri, L.C.; Simons, M. Metabolism and Functions of Lipids in Myelin. *Biochim. Biophys. Acta Mol. Cell Biol. Lipids* **2015**, *1851*, 999–1005. [CrossRef]
- 38. Di Gioacchino, M.; Bianconi, A.; Burghammer, M.; Ciasca, G.; Bruni, F.; Campi, G. Myelin Basic Protein Dynamics from Out-of-Equilibrium Functional State to Degraded State in Myelin. *Biochim. Biophys. Acta Biomembr.* **2020**, 1862, 183256. [CrossRef]

39. Frid, K.; Einstein, O.; Friedman-Levi, Y.; Binyamin, O.; Ben-Hur, T.; Gabizon, R. Aggregation of MBP in Chronic Demyelination. *Ann. Clin. Transl. Neurol.* **2015**, *2*, 711–721. [CrossRef] [PubMed]

- 40. Chen, C.; Han, D.; Cai, C.; Tang, X. An Overview of Liposome Lyophilization and Its Future Potential. *J. Control. Release* **2010**, 142, 299–311. [CrossRef] [PubMed]
- 41. Maleš, P.; Brkljača, Z.; Crnolatac, I.; Bakarić, D. Application of MCR-ALS with EFA on FT-IR Spectra of Lipid Bilayers in the Assessment of Phase Transition Temperatures: Potential for Discernment of Coupled Events. *Colloids Surf. B Biointerfaces* **2021**, 201, 111645. [CrossRef] [PubMed]
- 42. Menges, F. Spectragryph—Optical Spectroscopy Software. Available online: https://www.effemm2.de/spectragryph/ (accessed on 28 May 2025).
- 43. Pašalić, L.; Pem, B.; Bakarić, D. Lamellarity-Driven Differences in Surface Structural Features of DPPS Lipids: Spectroscopic, Calorimetric and Computational Study. *Membranes* **2023**, *13*, 83. [CrossRef]
- 44. Pem, B.; Brkljača, Z.; Philippe, A.; Schaumann, G.E.; Vazdar, M.; Bakarić, D. FTIR Spectroscopy and Molecular Level Insight of Diluted Aqueous Solutions of Acetic Acid. *Spectrochim. Acta Part A Mol. Biomol. Spectrosc.* **2023**, 302, 123135. [CrossRef]
- 45. BeStSelTM (2014–2023)—ELTE Eötvös Loránd University, Budapest, Hungary. Available online: https://bestsel.elte.hu/index.php (accessed on 8 May 2025).
- 46. Bamm, V.V.; De Avila, M.; Smith, G.S.T.; Ahmed, M.A.M.; Harauz, G. Structured Functional Domains of Myelin Basic Protein: Cross Talk between Actin Polymerization and Ca²⁺-Dependent Calmodulin Interaction. *Biophys. J.* **2011**, *101*, 1248–1256. [CrossRef] [PubMed]
- 47. Levine, Z.A.; Larini, L.; LaPointe, N.E.; Feinstein, S.C.; Shea, J.E. Regulation and Aggregation of Intrinsically Disordered Peptides. *Proc. Natl. Acad. Sci. USA* **2015**, *112*, 2758–2763. [CrossRef] [PubMed]
- 48. Garcia-Manyes, S.; Oncins, G.; Sanz, F. Effect of Ion-Binding and Chemical Phospholipid Structure on the Nanomechanics of Lipid Bilayers Studied by Force Spectroscopy. *Biophys. J.* **2005**, *89*, 1812–1826. [CrossRef]
- 49. De Vries, A.H.; Yefimov, S.; Mark, A.E.; Marrink, S.J. Molecular Structure of the Lecithin Ripple Phase. *Proc. Natl. Acad. Sci. USA* **2005**, *102*, 5392–5396. [CrossRef]
- 50. Böckmann, R.A.; Hac, A.; Heimburg, T.; Grubmüller, H. Effect of Sodium Chloride on a Lipid Bilayer. *Biophys. J.* **2003**, *85*, 1647–1655. [CrossRef]
- 51. Šegota, S.; Vojta, D.; Pletikapić, G.; Baranović, G. Ionic Strength and Composition Govern the Elasticity of Biological Membranes. A Study of Model DMPC Bilayers by Force- and Transmission IR Spectroscopy. *Chem. Phys. Lipids* **2015**, *186*, 17–29. [CrossRef]
- 52. Cevc, G. Polymorphism of the Bilayer Membranes in the Ordered Phase and the Molecular Origin of the Lipid Pretransition and Rippled Lamellae. *Biochim. Biophys. Acta Biomembr.* **1991**, 1062, 59–69. [CrossRef] [PubMed]
- 53. Heimburg, T. A Model for the Lipid Pretransition: Coupling of Ripple Formation with the Chain-Melting Transition. *Biophys. J.* **2000**, *78*, 1154–1165. [CrossRef]
- Mantsch, H.H.; Madec, C.; Lewis, R.N.; McElhaney, R.N. Thermotropic Phase Behavior of Model Membranes Composed of Phosphatidylcholines Containing Iso-Branched Fatty Acids. 2. Infrared and ³¹P NMR Spectroscopy Studies. *Biochemistry* 1985, 24, 2440–2446. [CrossRef] [PubMed]
- 55. Lewis, R.N.A.H.; McElhaney, R.N. Membrane Lipid Phase Transitions and Phase Organization Studied by Fourier Transform Infrared Spectroscopy. *Biochim. Biophys. Acta Biomembr.* **2013**, *1828*, 2347–2358. [CrossRef] [PubMed]
- 56. Casal, H.L.; Mantsch, H.H. The Thermotropic Phase Behavior of *N*-Methylated Dipalmitoylphosphatidylethanolamines. *Biochim. Biophys. Acta Biomembr.* **1983**, 735, 387–396. [CrossRef]
- 57. Cameron, D.G.; Casal, H.L.; Mantsch, H.H. Characterization of the Pretransition in 1,2-Dipalmitoyl-sn-Glycero-3-Phosphocholine by Fourier Transform Infrared Spectroscopy. *Biochemistry* **1980**, *19*, 3665–3672. [CrossRef]
- 58. Pašalić, L.; Pem, B.; Domazet Jurašin, D.; Vazdar, M.; Bakarić, D. Interaction of Guanidinium and Ammonium Cations with Phosphatidylcholine and Phosphatidylserine Lipid Bilayers—Calorimetric, Spectroscopic and Molecular Dynamics Simulations Study. *Biochim. Biophys. Acta Biomembr.* 2023, 1865, 184122. [CrossRef] [PubMed]
- 59. Maleš, P.; Munivrana, J.; Pašalić, L.; Pem, B.; Bakarić, D. Reorientation of Interfacial Water Molecules during Melting of Brain Sphingomyelin Is Associated with the Phase Transition of Its C24:1 Sphingomyelin Lipids. *Chem. Phys. Lipids* **2024**, 264, 105434. [CrossRef]
- 60. Maleš, P.; Nikšić-Franjić, I.; Wang, A.; Pem, B.; Bakarić, D. Optical and Molecular Features of Negatively Curved Surfaces Created by POPE Lipids: A Crucial Role of the Initial Conditions. *Spectrochim. Acta Part A Mol. Biomol. Spectrosc.* **2024**, *317*, 124462. [CrossRef]
- 61. Lewis, R.N.; McElhaney, R.N.; Pohle, W.; Mantsch, H.H. Components of the Carbonyl Stretching Band in the Infrared Spectra of Hydrated 1,2-Diacylglycerolipid Bilayers: A Reevaluation. *Biophys. J.* **1994**, *67*, 2367–2375. [CrossRef]
- 62. Steinbauer, B.; Mehnert, T.; Beyer, K. Hydration and Lateral Organization in Phospholipid Bilayers Containing Sphingomyelin: A

 2H-NMR Study. *Biophys. J.* **2003**, *85*, 1013–1024. [CrossRef]

63. Schmid, F. Physical Mechanisms of Micro- and Nanodomain Formation in Multicomponent Lipid Membranes. *Biochim. Biophys. Acta Biomembr.* **2017**, *1859*, 509–528. [CrossRef]

- 64. Bagatolli, L.A. To See or Not to See: Lateral Organization of Biological Membranes and Fluorescence Microscopy. *Biochim. Biophys. Acta Biomembr.* **2006**, *1758*, 1541–1556. [CrossRef] [PubMed]
- 65. Ramstedt, B.; Slotte, J.P. Membrane Properties of Sphingomyelins. FEBS Lett. 2002, 531, 33–37. [CrossRef]
- 66. Lewis, R.N.A.H.; McElhaney, R.N. Vibrational Spectroscopy of Lipids. In *Handbook of Vibrational Spectroscopy*; John Wiley & Sons, Ltd.: Hoboken, NJ, USA, 2006; pp. 3447–3464. ISBN 9780470027325.
- 67. Csiszár, A.; Koglin, E.; Meier, R.J.; Klumpp, E. The Phase Transition Behavior of 1,2-Dipalmitoyl-sn-Glycero-3-Phosphocholine (DPPC) Model Membrane Influenced by 2,4-Dichlorophenol—An FT-Raman Spectroscopy Study. Chem. Phys. Lipids 2006, 139, 115–124. [CrossRef]
- 68. Arsov, Z.; Quaroni, L. Detection of Lipid Phase Coexistence and Lipid Interactions in Sphingomyelin/Cholesterol Membranes by ATR-FTIR Spectroscopy. *Biochim. Biophys. Acta Biomembr.* **2008**, 1778, 880–889. [CrossRef]
- 69. Jiménez-Rojo, N.; García-Arribas, A.B.; Sot, J.; Alonso, A.; Goñi, F.M. Lipid Bilayers Containing Sphingomyelins and Ceramides of Varying *N*-Acyl Lengths: A Glimpse into Sphingolipid Complexity. *Biochim. Biophys. Acta Biomembr.* **2014**, *1838*, 456–464. [CrossRef] [PubMed]
- 70. Alavizargar, A.; Gass, M.; Krahn, M.P.; Heuer, A. Elucidating the Membrane Binding Process of a Disordered Protein: Dynamic Interplay of Anionic Lipids and the Polybasic Region. *ACS Phys. Chem. Au* **2024**, *4*, 167–179. [CrossRef] [PubMed]
- 71. Rispoli, P.; Carzino, R.; Svaldo-Lanero, T.; Relini, A.; Cavalleri, O.; Fasano, A.; Liuzzi, G.M.; Carlone, G.; Riccio, P.; Gliozzi, A.; et al. A Thermodynamic and Structural Study of Myelin Basic Protein in Lipid Membrane Models. *Biophys. J.* 2007, 93, 1999–2010. [CrossRef]
- 72. Min, Y.; Alig, T.F.; Lee, D.W.; Boggs, J.M.; Israelachvili, J.N.; Zasadzinski, J.A. Critical and Off-Critical Miscibility Transitions in Model Extracellular and Cytoplasmic Myelin Lipid Monolayers. *Biophys. J.* **2011**, *100*, 1490–1498. [CrossRef]
- 73. Benesch, M.G.K.; Lewis, R.N.A.H.; McElhaney, R.N. A Calorimetric and Spectroscopic Comparison of the Effects of Cholesterol and Its Sulfur-Containing Analogs Thiocholesterol and Cholesterol Sulfate on the Thermotropic Phase Behavior and Organization of Dipalmitoylphosphatidylcholine Bilayer Membranes. *Biochim. Biophys. Acta Biomembr.* **2016**, *1858*, 168–180. [CrossRef]
- 74. Chatterley, A.S.; Laity, P.; Holland, C.; Weidner, T.; Woutersen, S.; Giubertoni, G. Broadband Multidimensional Spectroscopy Identifies the Amide II Vibrations in Silkworm Films. *Molecules* **2022**, 27, 6275. [CrossRef]
- 75. de la Arada, I.; González-Ramírez, E.J.; Alonso, A.; Goñi, F.M.; Arrondo, J.L.R. Exploring Polar Headgroup Interactions between Sphingomyelin and Ceramide with Infrared Spectroscopy. *Sci. Rep.* **2020**, *10*, 17606. [CrossRef] [PubMed]
- 76. Wei, Y.; Thyparambil, A.A.; Latour, R.A. Protein Helical Structure Determination Using CD Spectroscopy for Solutions with Strong Background Absorbance from 190 to 230 Nm. *Biochim. Biophys. Acta Proteins Proteom.* **2014**, 1844, 2331–2337. [CrossRef] [PubMed]
- 77. Uversky, V.N. Paradoxes and Wonders of Intrinsic Disorder: Stability of Instability. *Intrinsically Disord. Proteins* **2017**, *5*, e1327757. [CrossRef]
- 78. Inoue, R.; Oda, T.; Nakagawa, H.; Tominaga, T.; Ikegami, T.; Konuma, T.; Iwase, H.; Kawakita, Y.; Sato, M.; Sugiyama, M. Revealing an Origin of Temperature-Dependent Structural Change in Intrinsically Disordered Proteins. *Biophys. J.* 2025, 124, 540–548. [CrossRef]
- 79. Balleza, D.; Mescola, A.; Marín–Medina, N.; Ragazzini, G.; Pieruccini, M.; Facci, P.; Alessandrini, A. Complex Phase Behavior of GUVs Containing Different Sphingomyelins. *Biophys. J.* **2019**, *116*, 503–517. [CrossRef]
- 80. Krugmann, B.; Radulescu, A.; Appavou, M.S.; Koutsioubas, A.; Stingaciu, L.R.; Dulle, M.; Förster, S.; Stadler, A.M. Membrane Stiffness and Myelin Basic Protein Binding Strength as Molecular Origin of Multiple Sclerosis. *Sci. Rep.* **2020**, *10*, 16691. [CrossRef]
- 81. Has, C.; Sivadas, P.; Das, S.L. Insights into Membrane Curvature Sensing and Membrane Remodeling by Intrinsically Disordered Proteins and Protein Regions. *J. Membr. Biol.* **2022**, 255, 237–259. [CrossRef]
- 82. Akbayrak, I.Y.; Caglayan, S.I.; Ozcan, Z.; Uversky, V.N.; Coskuner-Weber, O. Current Challenges and Limitations in the Studies of Intrinsically Disordered Proteins in Neurodegenerative Diseases by Computer Simulations. *Curr. Alzheimer Res.* 2020, 17, 805–818. [CrossRef] [PubMed]
- 83. Gil Pineda, L.I.; Milko, L.N.; He, Y. Performance of CHARMM36m with Modified Water Model in Simulating Intrinsically Disordered Proteins: A Case Study. *Biophys. Rep.* **2020**, *6*, 80–87. [CrossRef]
- 84. Wang, W. Recent Advances in Atomic Molecular Dynamics Simulation of Intrinsically Disordered Proteins. *Phys. Chem. Chem. Phys.* **2021**, 23, 777–784. [CrossRef]
- 85. Majewski, J.; Jones, E.M.; Vander Zanden, C.M.; Biernat, J.; Mandelkow, E.; Chi, E.Y. Lipid Membrane Templated Misfolding and Self-Assembly of Intrinsically Disordered Tau Protein. *Sci. Rep.* **2020**, *10*, 13324. [CrossRef]
- 86. El Mammeri, N.; Gampp, O.; Duan, P.; Hong, M. Membrane-Induced Tau Amyloid Fibrils. *Commun. Biol.* **2023**, *6*, 467. [CrossRef] [PubMed]

87. Ivankov, O.; Murugova, T.N.; Ermakova, E.V.; Kondela, T.; Badreeva, D.R.; Hrubovčák, P.; Soloviov, D.; Tsarenko, A.; Rogachev, A.; Kuklin, A.I.; et al. Amyloid-Beta Peptide (25–35) Triggers a Reorganization of Lipid Membranes Driven by Temperature Changes. *Sci. Rep.* **2021**, *11*, 21990. [CrossRef] [PubMed]

- 88. Chakraborty, S.; Doktorova, M.; Molugu, T.R.; Heberle, F.A.; Scott, H.L.; Dzikovski, B.; Nagao, M.; Stingaciu, L.R.; Standaert, R.F.; Barrera, F.N.; et al. How Cholesterol Stiffens Unsaturated Lipid Membranes. *Proc. Natl. Acad. Sci. USA* **2020**, *117*, 21896–21905. [CrossRef] [PubMed]
- 89. Träger, J.; Widder, K.; Kerth, A.; Harauz, G.; Hinderberger, D. Effect of Cholesterol and Myelin Basic Protein (MBP) Content on Lipid Monolayers Mimicking the Cytoplasmic Membrane of Myelin. *Cells* **2020**, *9*, 529. [CrossRef]

Disclaimer/Publisher's Note: The statements, opinions and data contained in all publications are solely those of the individual author(s) and contributor(s) and not of MDPI and/or the editor(s). MDPI and/or the editor(s) disclaim responsibility for any injury to people or property resulting from any ideas, methods, instructions or products referred to in the content.